CMS Physics Analysis Summary

Contact: cms-pag-conveners-higgs@cern.ch 2018/07/24

A search for pair production of new light bosons decaying into muons at $\sqrt{s} = 13$ TeV

The CMS Collaboration

Abstract

This letter presents a search for new light bosons decaying into muon pairs using a data sample corresponding to an integrated luminosity of 35.9 fb^{-1} of proton-proton collisions at a center-of-mass energy $\sqrt{s} = 13$ TeV collected with the CMS detector at the CERN LHC. The search is model independent, only requiring the pair production of a new light boson and its subsequent decay to a pair of muons. No significant deviation is observed from the predicted background and a model independent limit is set on the product of the cross section, branching ratio, and acceptance as a function of mass. This limit varies between 0.16 fb and 0.45 fb over a range of new light boson masses from 0.25 GeV to 8.5 GeV. It is then interpreted in the context of the Next-to-Minimal Supersymmetric Standard Model and a dark supersymmetry model that allows for non-negligible light boson lifetimes.

1 Introduction

The Standard Model of particle physics (SM) is known to be an incomplete description of physics and a number of extensions of the SM predict the production of new light bosons [1–3]. In this Letter we present a model independent search for the pair production of a light boson that decays to a pair of muons. A simple example of such a decay channel is $pp \to h \to 2a + X \to 4\mu + X$, where h is a Higgs boson (either SM or non-SM), a is a new light boson, and X are spectator particles which are predicted in some models [4]. While decay from a Higgs boson is possible, it is not required in the search presented here: the only requirement is that a pair of identical light bosons be created at a common vertex and each light boson subsequently decays to a pair of muons. These muon pairs are referred to as "dimuons"; the dimuon and new light boson production vertexes are allowed to be displaced. The generic nature of this signature means that any limit set on the product of the cross section, branching ratio, and acceptance is model-independent; it can thus be reinterpreted in the context of specific models.

To help ensure model independence, two different classes of benchmark models were used to design the analysis and interpret the results: the next-to-minimal supersymmetric standard model (NMSSM) [1, 5–12] and supersymmetry (SUSY) models with hidden sectors [3, 13, 14] (dark SUSY). In the NMSSM benchmark models, two of the three CP-even neutral Higgs bosons h_1 or h_2 can decay to one of the two CP-odd neutral Higgs bosons via $h_{1,2} \to 2a_1$. The light boson a_1 subsequently decays to a pair of oppositely charged muons. In the dark SUSY benchmark models, the breaking of a new $U(1)_D$ symmetry (where the subscript "D" means "Dark") gives rise to a massive dark photon γ_D. This dark photon can couple to SM particles via a small kinetic mixing ε with SM photons. The lifetime, and thus displacement, of a dark photon is dependent upon m_{γ_D} and ε. The topologies investigated feature an SM-like Higgs boson h that decays via $h \to 2n_1$, where n_1 is the lightest non-dark neutralino. The n_1 then each decay via $n_1 \to n_D + \gamma_D$, where n_D is a dark neutralino that is undetected. The dark photon γ_D decays to a pair of oppositely charged muons. This analysis contributes to an existing body of experimental work in the search for new light bosons. Previous searches at the LHC for $h \to 2a$ include those with final states that feature 4μ [15–17], 4τ [18], 4ℓ [19, 20], $4\ell/4\pi$ [21], 4b [22, 23], 4γ [24], 2b 2τ [25], 2μ 2τ [26], and 6q [27]. A more thorough description of these models, their empirical and theoretical motivations, and constraints for this search set by previous experiments is included in Refs. [15] and [28].

The search presented in this Letter includes several improvements compared to the previous results published by CMS on light boson pair production decaying to muons given in Ref. [15]. The data used for the analysis correspond to $35.9\,\text{fb}^{-1}$ collected at a center-of-mass energy of $\sqrt{s} = 13\,\text{TeV}$ rather than $20.7\,\text{fb}^{-1}$ at 8 TeV. A triple-muon trigger with no constraint on the dimuon vertex has replaced the previous double-muon triggers, increasing the sensitivity to displaced signatures. Improvements were made to the CMS detector including the installation of additional Resistive Plate Chambers (RPCs) and Cathode Strip Chambers (CSCs) in the outer layer of the CMS endcap muon system; these improvements are discussed in detail in Ref. [29]. The analysis criteria were improved to enhance the sensitivity of the search for a new light boson a_1 with a mass between 0.25 to 3.55 GeV in the context of NMSSM benchmark models and a dark photon γ_D with a mass in between 0.25 to 8.5 GeV and lifetime up to $c\tau_{\gamma_D} = 100\,\text{mm}$ in the context of benchmark dark SUSY models. These changes lead to greater detection sensitivity and coverage of model parameter space.

2 The CMS Detector

The central feature of the CMS apparatus is a superconducting solenoid of 6 m internal diameter, providing a magnetic field of 3.8 T. Within the solenoid volume are a silicon pixel and strip tracker, a lead tungstate crystal electromagnetic calorimeter, and a brass and scintillator hadron calorimeter, each composed of a barrel and two endcap sections. Forward calorimeters extend the pseudorapidity coverage provided by the barrel and endcap detectors. Muons are detected in gas-ionization chambers embedded in the steel flux-return yoke outside the solenoid.

Muons are measured in the pseudorapidity range $|\eta| < 2.4$, with detection planes made using three technologies: drift tubes, CSCs, and RPCs. Matching muons to tracks measured in the silicon tracker results in a relative transverse momentum (p_T) resolution for muons with $20 < p_T < 100$ GeV of 1.3–2.0% in the barrel and better than 6% in the endcaps. The p_T resolution in the barrel is better than 10% for muons with p_T up to 1 TeV [30].

Events of interest are selected using a two-tiered trigger system [31]. The first level (L1), composed of custom hardware processors, uses information from the calorimeters and muon detectors to select events at a rate of around 100 kHz within a time interval of less than 4 μs. The second level, known as the high-level trigger (HLT), consists of a farm of processors running a version of the full event reconstruction software optimized for fast processing, and reduces the event rate below 1 kHz before data storage.

A more detailed description of the CMS detector, together with definitions of the coordinate system used and the relevant kinematic variables, can be found in Ref. [32].

3 Data selection

The data were collected with a trigger that uses muon reconstruction algorithms optimized for vertexes displaced from the primary vertex by as much as 9.8 cm in the plane transverse to the beam line. The HLT is seeded by requiring the presence of two L1 muons in an event, the leading muon with $p_T > 12$ GeV, the sub-leading muon with $p_T > 5$ GeV and both satisfying $|\eta| < 2.4$. Events that later pass the HLT are required to have at least three reconstructed muons, one with $p_T > 15$ GeV and $|\eta| < 2.4$ and the other two with $p_T > 5$ GeV and $|\eta| < 2.4$. Events selected with this trigger are then reconstructed with the Particle-Flow (PF) algorithm, which reconstructs the final-state particles using a global fit that combines the information from each subdetector [33].

The offline event selection in this analysis requires events to have a primary vertex reconstructed using a Kalman Filtering (KF) technique [34]. In addition, each event contains at least four muons reconstructed with the PF algorithm and identified as PF muons or as muons found in the tracker. Each muon is required to have $p_T > 8$ GeV and $|\eta| < 2.4$. At least one muon must be a "high-p_T" muon, i.e. it must be found in the barrel region ($|\eta| < 0.9$) and must have $p_T > 17$ GeV in order to ensure that the trigger reconstruction has no dependency on η.

"Dimuons" are constructed from pairs of oppositely charged muons that share a common vertex, reconstructed using a KF technique, and must have an invariant mass $m_{(\mu\mu)}$ less than 9 GeV. Exactly two dimuons must be present in each event. A dimuon that contains a high-p_T muon is called a "high-p_T dimuon". When only one high-p_T muon is present in the event, the high-p_T dimuon is denoted as $(\mu\mu)_1$, while the other as $(\mu\mu)_2$. When both dimuons have at least one high-p_T muon, the dimuons are labeled randomly. Single muons not included in dimuons are called "orphan" muons. No cut is applied on the number of orphan muons. Each dimuon must have at least one hit reconstructed in the pixel system. The dimuons are required to

originate from the same primary vertex, $|z_{(\mu\mu)_1} - z_{(\mu\mu)_2}| < 0.1$ cm, where $z_{(\mu\mu)}$ denotes the z position of the secondary vertex associated with the dimuon propagated back to the beam-line along the dimuon direction vector. Furthermore, each dimuon must be sufficiently isolated. The dimuon isolation $I_{(\mu\mu)}$ is calculated as the sum of the transverse momenta of tracks with at least $p_T > 0.5$ GeV in the vicinity of the dimuon within $\Delta R < 0.4$ and $|z_{\text{track}} - z_{(\mu\mu)}| < 0.1$ cm. Here ΔR is defined in terms of the track separation in pseudorapidity (η) and azimuthal angle (ϕ) as $\Delta R = \sqrt{(\Delta\eta)^2 + (\Delta\phi)^2}$, while z_{track} is defined as the z coordinate of the point of closest approach to the primary vertex along the beam axis. Tracks included in the dimuon reconstruction are excluded from the isolation calculation. The total isolation sum must be less than 2 GeV. Since the dimuons are expected to originate from the same type of light bosons, the dimuon masses should be consistent to within five times the detector resolution, i.e. $|m_{(\mu\mu)_1} - m_{(\mu\mu)_2}| < 0.13 + 0.065(m_{(\mu\mu)_1} + m_{(\mu\mu)_2})/2$. This requirement carves out a signal region in the two dimensional plane of the dimuon invariant masses $m_{(\mu\mu)_1}$ and $m_{(\mu\mu)_2}$.

Scale factors are determined to correct for differences between observed data and simulated samples. Corrections for the identification and isolation of muons and isolation of dimuons are measured using $Z \to \mu^-\mu^+$ and $J/\psi \to \mu^-\mu^+$ samples using a "tag and probe" technique; the samples used are events from simulated data and from observed data control regions enriched in events from the aforementioned SM processes. All muons in these samples are required to have $p_T > 8$ GeV, the "tag" muon is required to be a loose muon as described in Ref. [29], while the "probe" muon criteria varies according to the variable under study. Corrections for the trigger efficiency are extracted using $WZ \to 3\mu$ and $t\bar{t}Z \to 3\mu$ events that are also extracted from simulated data samples and enriched observed data samples; these samples are selected using a missing transverse energy requirement such that they do not contain events in common with the data sample used in this analysis. A scale factor per event $\epsilon_{\text{Data}}/\epsilon_{\text{Sim}} = 0.93 \pm 0.06$ is obtained. For future interpretation of the results in Section 7 a parameter $\bar{r}$ is defined as the ratio of the full efficiency over the generator level acceptance, including a data to MC scale factor, averaged over all MC signal samples, and is found to be $\bar{r} = 0.56 \pm 0.06$.

4 Signal modeling

Proton-proton collisions at $\sqrt{s} = 13$ TeV were simulated for samples in each of the two benchmark models, NMSSM and dark SUSY. The parton distribution functions were modeled using NNPDF2.3LO [35]. The underlying event activity at the LHC and jet fragmentation were modeled with PYTHIA [36] using the "Monash" tune [37]. Specifically, PYTHIA 8.212 was used for NMSSM and PYTHIA 8.205 for dark SUSY. In each model, only Higgs boson production through gluon-gluon fusion was considered. A single mass point was also generated through vector boson fusion (VBF) and associated vector boson production (VH) to determine their contribution to the $h_2 \to 2a_1$ cross section; this is included in a simplified reference scenario discussed later.

In the case of NMSSM, the simulated Higgs boson h_2 is forced to decay to a pair of light bosons a_1, each subsequently decaying to a pair of oppositely charged muons. Since the h_2 in $h_2 \to 2a_1$ might not be the observed h (125), m_{h_2} between 90 and 150 GeV were simulated. This range is motivated by constraints set by relic density measurements from WMAP [38] and Planck [39] as well as searches at LEP [40–45]. The light boson mass was simulated to vary between $2m_\mu$ and $2m_\tau$, or between 0.25 GeV and 3.55 GeV as motivated in Ref [46].

In the case of dark SUSY, production of SM Higgs bosons was simulated with MadGraph 4.5.2 [47]. The non-SM decay of the Higgs bosons was modeled using the BRIDGE program [48]. Higgs bosons were forced to decay to a pair of n_1 SUSY neutralinos, $h \to 2n_1$. Each SUSY neutralino in turn decays to a dark photon and a dark neutralino $n_1 \to n_D + \gamma_D$. The

dark neutralinos are considered stable and escape detection. We set the dark photons to decay to a pair of oppositely charged muons 100% of the time, $\gamma_D \to \mu^-\mu^+$. The Higgs boson mass and n_1 mass were fixed to 125 GeV and 10 GeV, respectively. Dark photon masses m_{γ_D} were simulated between 0.25 GeV and 8.5 GeV. The width of the dark photons was set to 10^{-3} GeV. Muon displacement was modeled with an exponential distribution with $c\tau_{\gamma_D}$ between 0 mm and 100 mm. All Monte Carlo generated events were run through the full CMS simulation based on GEANT4 [49] and reconstructed using CMS software.

One of the key features of this analysis is the model independence of the results. This is ensured by verifying that the ratio of the full reconstruction efficiency ϵ_{Full} over the generator level acceptance α_{Gen} is independent of the signal model. The signal acceptance is defined as the fraction of Monte Carlo generated events that pass the generator level selection criteria. The criteria are as follows: at least four muons in each event with $p_{\text{T}} > 8$ GeV and $|\eta| < 2.4$, at least one muon with $p_{\text{T}} > 17$ GeV and $|\eta| < 0.9$, and both dark bosons must have a transverse decay length $L_{xy} < 9.8$ cm and longitudinal decay length $|L_z| < 46.5$ cm. ϵ_{Full} is defined as the fraction of Monte Carlo generated events that pass the trigger and full offline selection described above. The model independence is illustrated in Table 1 for several representative signal models.

Table 1: The full reconstruction efficiency over signal acceptance $\epsilon_{\text{Full}}/\alpha_{\text{Gen}}$ in % for several representative signal NMSSM (top) and dark SUSY benchmark models (bottom).

m_{h_1} [GeV]	90	100	110	125	150
m_{a_1} [GeV]	2	0.5	3	1	0.75
ϵ_{Full} [%]	8.85 ± 0.06	13.23 ± 0.08	11.96 ± 0.07	14.68 ± 0.08	18.48 ± 0.09
α_{Gen} [%]	13.93 ± 0.08	20.47 ± 0.09	19.24 ± 0.09	23.59 ± 0.10	29.93 ± 0.10
$\epsilon_{\text{Full}}/\alpha_{\text{Gen}}$ [%]	63.52 ± 0.29	64.62 ± 0.24	62.19 ± 0.25	62.23 ± 0.22	61.73 ± 0.20

m_{γ_D} [GeV]	0.25			8.5		
$c\tau_{\gamma_D}$ [mm]	0	1	5	0	2	20
ϵ_{Full} [%]	9.12 ± 0.21	1.72 ± 0.06	0.12 ± 0.01	12.78 ± 0.12	12.25 ± 0.06	3.61 ± 0.02
α_{Gen} [%]	13.52 ± 0.25	2.85 ± 0.07	0.20 ± 0.01	20.49 ± 0.14	20.05 ± 0.08	6.16 ± 0.03
$\epsilon_{\text{Full}}/\alpha_{\text{Gen}}$ [%]	67.47 ± 0.91	60.2 ± 1.3	58.39 ± 2.0	62.36 ± 0.38	61.10 ± 0.21	58.70 ± 0.24

5 Background estimation

The selection criteria described in Section 3 is effective at reducing and eliminating most SM backgrounds with similar topology to our signal. As a result, this analysis is expected to have a very small background contribution in the signal region (SR). Three SM backgrounds were found to be non-negligible and are presented here: b-quark pair production ($b\bar{b}$), prompt double J/ψ, and electroweak production of four muons. Contributions from Y mesons were also considered; they were found to be negligible below the 8.5 GeV upper bound on m_a. The total background contribution in the signal region was estimated to be $9.90 \pm 1.24\,(\text{stat}) \pm 1.84\,(\text{syst})$ events; the contributions from each process are described below.

5.1 The $b\bar{b}$ background

The largest background, $b\bar{b}$ production, is dominated by events in which both b quarks decay to $\mu^+\mu^- + X$ or go through low-mass meson resonances such as ω, ρ, ϕ, J/ψ, ψ. The J/ψ contribution considered in this background is non-prompt; the prompt J/ψ contribution is considered

in Section 5.2. A minor contribution comes from events with charged tracks misidentified as muons. A two-dimensional template, $S(m_{(\mu\mu)_1}, m_{(\mu\mu)_2})$, was constructed in the plane of the two dimuon invariant masses and used to estimate the contribution to the SM background from $\mathrm{b\bar{b}}$ decays. The construction of this background template is described as follows.

First, a $\mathrm{b\bar{b}}$-enriched control sample was selected from events with similar kinematic properties as the signal events, but not included in the signal region. Events were required to pass the signal trigger and have exactly three muons. One of these muons must have $p_\mathrm{T} > 17\,\mathrm{GeV}$ within $|\eta| < 0.9$, while the other two have $p_\mathrm{T} > 8\,\mathrm{GeV}$ within $|\eta| < 2.4$. In addition, the control region selection requires a good primary vertex, exactly one dimuon, and one orphan muon. The longitudinal distance between the projections of the dimuon trajectory starting from its vertex and the orphan muon track back to the beam axis, $\Delta z((\mu\mu), \mu_\mathrm{orphan})$ must have an absolute value less than 0.1 cm. The dimuon is required to have at least one hit in the pixel system as explained in Section 3. Finally, the dimuon isolation value can be no higher than 2 GeV. The requirements on the $\mathrm{b\bar{b}}$-enriched events ensure that the template can be extrapolated into the signal region.

Next, two one-dimensional templates, $S_\mathrm{I}(m_{(\mu\mu)})$ and $S_\mathrm{II}(m_{(\mu\mu)})$, are obtained separately from the $\mathrm{b\bar{b}}$-enriched events. In the case of $S_\mathrm{I}(m_{(\mu\mu)})$, at least one high-$p_\mathrm{T}$ muon is contained in the dimuon. In the case of $S_\mathrm{II}(m_{(\mu\mu)})$, the high-$p_\mathrm{T}$ muon is the orphan muon and the dimuon may or may not contain another high-p_T muon. This procedure ensures that kinematic differences between signal events that have exactly two high-p_T dimuons or just one high-p_T dimuon are taken into account. Each distribution was fitted with a shape comprised of a Gaussian distribution for each light meson resonance, a double-sided Crystal Ball function for the J/ψ peak, and a set of sixth degree Bernstein polynomials for the bulk shape. The template $S(m_{(\mu\mu)_1}, m_{(\mu\mu)_2})$ was obtained as $S_\mathrm{I}(m_{(\mu\mu)}) \otimes S_\mathrm{II}(m_{(\mu\mu)})$, where $\otimes$ represents the Cartesian product.

Finally, the two-dimensional template was then normalized in the dimuon-dimuon mass space from 0.25 to 8.5 GeV. The ratio between the area of the template in the diagonal A_D and the off-diagonal region A_OD shown in Fig. 1 was calculated to be $R = A_\mathrm{D}/A_\mathrm{OD} = 0.141/0.859$. This scale factor was used to extrapolate the number of $\mathrm{b\bar{b}}$ events in the off-diagonal region, shown as the 56 white circles in Fig. 1, to the diagonal region (corridor). The number of $\mathrm{b\bar{b}}$ events in the corridor was estimated to be $R \times (56 \pm \sqrt{56}) = 9.21 \pm 1.23$.

This method of estimating the $\mathrm{b\bar{b}}$ contribution to background events was further validated by repeating the procedure for different values for the dimuon isolation (5, 10, 50 GeV) and without any isolation. The $\mathrm{b\bar{b}}$ event yield was stable in the signal region within 20%, which was assigned as a systematic uncertainty.

5.2 Prompt double J/ψ background

Two mechanisms contribute to prompt double J/ψ production: single parton scattering (SPS) and double parton scattering (DPS). They can mimic the signal process when each J/ψ meson decays to a pair of muons with opposite charge. The prompt double J/ψ background is estimated with a method that uses both experimental and simulated data. In a control sample of experimental data, the prompt and non-prompt double J/ψ contributions are separated using the "ABCD" method (see description in Ref. [50]). The prompt contribution is then extrapolated into the signal region. Double J/ψ events are selected with a trigger dedicated for b-physics. Each event is required to have at least four muons with $p_\mathrm{T} > 3.5\,\mathrm{GeV}$ within $|\eta| < 2.4$. No high-p_T muon is required. Events must have exactly two dimuons, with labels $(\mu\mu)_1$ or $(\mu\mu)_2$ assigned randomly to prevent a bias in kinematic distributions. The dimuon isolation follows the same definition as in Sec. 3, but no cut is applied. The kinematic properties of SPS and

DPS were studied using Monte Carlo simulation. SPS and DPS events were generated using PYTHIA 8.2 [51] and HERWIG 2.7.1 [52]. The variable with the most SPS-DPS separation power was found to be the absolute difference in rapidity between the two dimuons, $|\Delta y|$. To remove non-resonant muon pairs from the sample, the dimuon masses were required to be within 2.8 and 3.3 GeV. The ABCD method was then employed using the dimuon isolations as uncorrelated variables in the plane $(I_{(\mu\mu)_1}, I_{(\mu\mu)_2})$. The maximum isolation on $(\mu\mu)_1$ and $(\mu\mu)_2$ was set to 12 GeV. Here, region "A" is the region bounded by $I_{(\mu\mu)_{1,2}} < 2$ GeV. Conversely, "B", "C", and "D" are non-isolated sideband regions used to extrapolate the non-prompt contribution into region "A". The non-prompt $|\Delta y|$ distribution is determined from the sideband regions; this distribution was scaled to match the non-prompt contribution in region "A". This is then subtracted from $|\Delta y|$, leaving the prompt $|\Delta y|$ in region "A". To separate the prompt SPS from prompt DPS in the data, a template distribution $f_{\mathrm{SPS}}|\Delta y_{\mathrm{SPS}}| + (1 - f_{\mathrm{SPS}})|\Delta y_{\mathrm{DPS}}|$ was fitted to the corresponding $|\Delta y|$ distribution in data, where f_{SPS} and $1 - f_{\mathrm{SPS}}$ are the fractions of prompt SPS and DPS events, respectively. Finally, this result is used to determine the number of events that are expected in the SR of our experimental data sample. The contribution of the prompt double J/ψ events in data passing the signal selections in Section 3 was then calculated to be $N_{\mathrm{data}}(SR) = 0.33 \pm 0.08$.

5.3 Electroweak background

Electroweak production of four muons, $\mathrm{pp} \to 4\mu$, was estimated using Monte Carlo events generated with CALCHEP 3.6.25 [53]. The processes studied include $\mathrm{q\bar{q}} \to \mathrm{ZZ}^* \to 2\mu^+2\mu^-$ and $\mathrm{q\bar{q}} \to \mathrm{Z} \to \mu^+\mu^-$, where one of the muons radiates a second Z which decays to a $\mu^+\mu^-$ pair. Other electroweak processes, such as $\mathrm{pp} \to \mathrm{h}(125) \to \mathrm{ZZ}^* \to 2\mu^+2\mu^-$, were determined to be negligible a priori and thus are not included. Based on the simulation, the electroweak background was found to be 0.36 ± 0.09. Unlike the prompt double J/ψ background, the electroweak background is not concentrated at any particular mass value; its contribution to any mass bin is negligible compared to the $\mathrm{b\bar{b}}$ background. For this reason, these background events are neglected in any limit setting computation.

6 Systematic uncertainties

Both instrumental and theoretical sources of uncertainty are considered in this section. The significant sources of instrumental uncertainty are the muon trigger efficiency (6%), the uncertainty in the measurement of the integrated luminosity recorded by CMS (2.5%) [54], the muon identification data to simulation scale factor (0.6% per muon), the reconstruction of the dimuon in the tracker (1.2% per dimuon) and the muon system (1.3% per dimuon) from spatially close muons, and the effect on the acceptance of the dimuon mass shape used to determine the width of the signal region (1.5%). The uncertainty in the dimuon isolation and pileup are determined to be negligible.

The theoretical uncertainties are dominated by the uncertainty in the parton distribution functions (PDF), knowledge of the strong coupling constant α_S, and the QCD renormalization and factorization scales. The PDF and α_S uncertainties are estimated using a technique that follows the PDF4LHC recommendations [55–58]. The uncertainty in the scale factors is determined by varying μ_{R} and μ_{F} up and down by a factor of two using MCFM [59]. The effect of PDF choice and PDF parameter variation upon the central values is also studied. When all previously described theoretical uncertainties are added in quadrature, the sum is 8%. Systematic errors on the total signal cross section for each production mechanism and for all Higgs boson masses are fully defined in Ref. [60]. The cross section uncertainties are treated as uncorrelated and a

total systematic uncertainty of 3.2% is assigned to the signal cross section. The uncertainty in the branching fraction is taken to be 2%.

7 Results

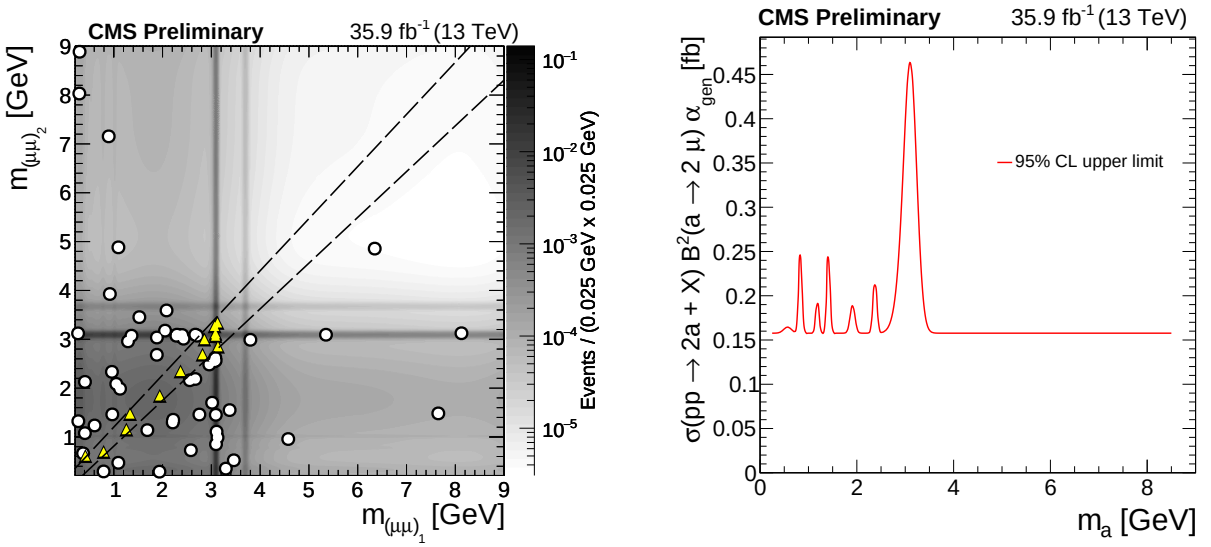

Figure 1: Left: The distribution of the invariant masses $m_{(\mu\mu)_1}$ vs. $m_{(\mu\mu)_2}$ for the isolated dimuon systems. There are 56 events in the data (bullets) that pass all selection criteria except for the $m_{(\mu\mu)_1} \simeq m_{(\mu\mu)_2}$ requirement and thus fall outside the diagonal region. The diagonal signal region $m_{(\mu\mu)_1} \simeq m_{(\mu\mu)_2}$ (outlined with dashed lines) contains the 13 events observed in data (triangles) that pass all selection criteria. The expected SM background distribution is indicated by the color scale. Right: The 95% CL upper limit set on $\sigma(\mathrm{pp} \to 2\mathrm{a} + \mathrm{X}) \times \mathcal{B}^2(\mathrm{a} \to 2\mu) \times \alpha_{\mathrm{Gen}}$ over the range $0.25 < m_{\mathrm{a}} < 8.5\,\mathrm{GeV}$.

After applying all selection criteria to the data sample, 13 events are found in the signal region. This result is consistent with the $9.90 \pm 1.24\,(\mathrm{stat}) \pm 1.84\,(\mathrm{syst})$ events predicted from the background estimate described in Section 5. These events can be seen in Fig. 1 (left); their distribution is consistent with the expected background displayed on the same figure. A model independent 95% confidence level (CL) upper limit is set on the product branching fraction $\sigma(\mathrm{pp} \to 2\mathrm{a} + \mathrm{X}) \times \mathcal{B}^2(\mathrm{a} \to 2\mu) \times \alpha_{\mathrm{Gen}} \leq N(m_{(\mu\mu)})/(\mathcal{L}\bar{r})$, using the modified frequentist procedure that incorporates individual uncertainties and their correlations. Here $\bar{r}$ is the parameter introduced in Section 3 averaged over all MC signal samples and $\mathcal{L}$ is the integrated luminosity of $35.9\,\mathrm{fb}^{-1}$. This limit is shown as a function of m_{a} in Fig. 1 (right) and can be interpreted in the context of specific models.

For the NMSSM scenario, the 95% CL upper limit is derived for $\sigma\,(\mathrm{pp} \to \mathrm{h}_{1,2} \to 2\mathrm{a}_1) \times \mathcal{B}^2(\mathrm{a}_1 \to 2\mu)$ as a function of $m_{\mathrm{h}_{1,2}}$ for two choices of m_{a_1} as shown in Fig. 2 (left) and as a function of m_{a_1} for three choices of m_{h_1} as shown in Fig. 2 (right). Since the choice of m_{h_1} does not restrict m_{h_2}, we choose to set $\varepsilon_{\mathrm{Full}}(m_{\mathrm{h}_2}) = \varepsilon_{\mathrm{Full}}(m_{\mathrm{h}_1})$ to simplify the expression. This choice is conservative because $\varepsilon_{\mathrm{Full}}(m_{\mathrm{h}_2}) > \varepsilon_{\mathrm{Full}}(m_{\mathrm{h}_1})$ if $m_{\mathrm{h}_2} > m_{\mathrm{h}_1}$, for any m_{a_1}. In this simplified prediction scenario, $\mathcal{B}(\mathrm{a}_1 \to 2\mu)$ is a function of m_{a_1} as calculated in [46]. We include a reference line where the ratio of the vacuum expectation values of the Higgs doublets $\tan\beta$ is set to 20 in both Fig. 2 left and right. We set $\mathcal{B}(\mathrm{h}_1 \to 2\mathrm{a}_1)$ to 0.3% so that the resulting reference lines are similar to the upper limits that are determined from the yield of dimuon pair events observed in the data. In Fig. 2 (left), the representative value of $\mathcal{B}(\mathrm{a}_1 \to 2\mu)$ is equal to 7.7% for $m_{\mathrm{a}_1} \approx 2$ GeV. In the

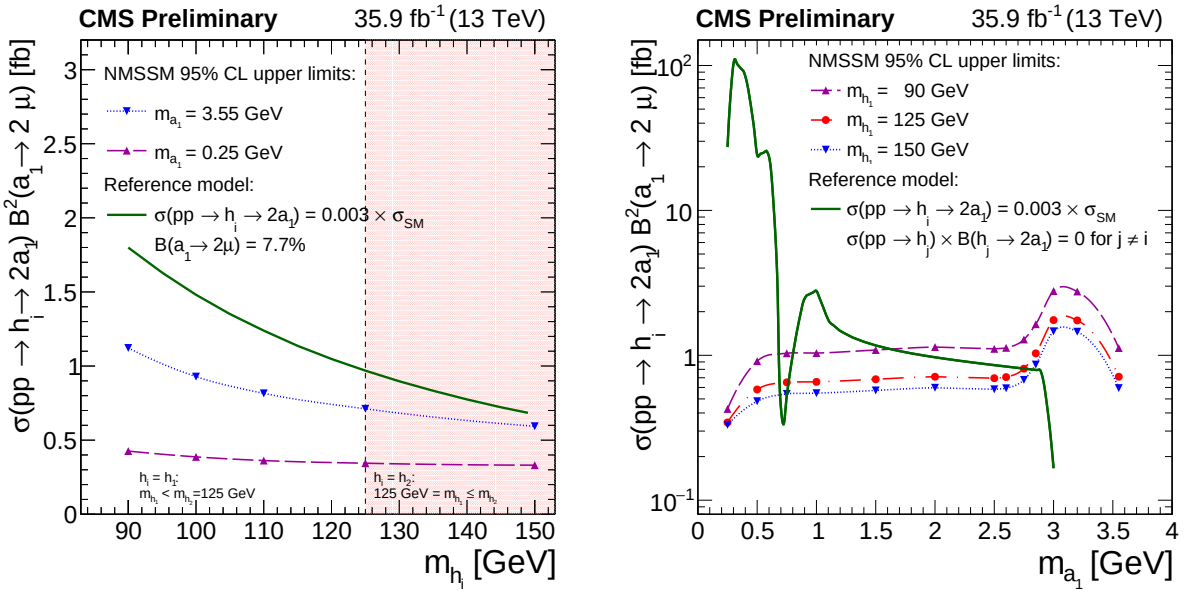

Figure 2: Left: The 95% CL upper limits in the NMSSM scenario as functions of m_{h_1} on $\sigma(pp \to h_{1,2} \to 2a_1) \times \mathcal{B}^2(a_1 \to 2\mu)$ with $m_{a_1} = 0.25\,\text{GeV}$ (dashed curve) and $m_{a_1} = 3.55\,\text{GeV}$ (dotted curve). The limits are compared to a representative predicted rate (solid curve) obtained using a simplified scenario where $\sigma(pp \to h_1) = \sigma_{SM}(m_{h_1})$ [60], $\sigma(pp \to h_2) \times \mathcal{B}(h_2 \to 2a_1) = 0$, $\mathcal{B}(h_1 \to 2a_1) = 0.3\%$, and $\mathcal{B}(a_1 \to 2\mu) = 7.7\%$. For the chosen $\mathcal{B}(a_1 \to 2\mu)$, taken from [46], $m_{a_1} = 2\,\text{GeV}$ and NMSSM parameter $\tan\beta = 20$. The figure is separated into two regions: $m_{h_i} = m_{h_1} < 125$ GeV with $m_{h_2} = 125$ GeV (unshaded), and $m_{h_1} = 125$ GeV with $m_{h_i} = m_{h_2} > 125$ GeV (shaded). Right: The 95% CL upper limits as functions of m_{a_1} in the NMSSM scenario on $\sigma(pp \to h_{1,2} \to 2a_1) \times \mathcal{B}^2(a_1 \to 2\mu)$ with $m_{h_1} = 90\,\text{GeV}$ (dashed curve), $m_{h_1} = 125\,\text{GeV}$ (dash-dotted curve), and $m_{h_1} = 150\,\text{GeV}$ (dotted curve). These limits are compared to a representative predicted rate (solid curve) from a simplified case in which $\mathcal{B}(h_1 \to 2a_1) = 0.3\%$, $\sigma(pp \to h_1) = \sigma_{SM}(m_{h_1} = 125\,\text{GeV})$ [60], and $\sigma(pp \to h_2) \times \mathcal{B}(h_2 \to 2a_1) = 0$. Additionally, $\mathcal{B}(a_1 \to 2\mu)$ as a function of m_{a_1} is taken from [46] and assumes that the NMSSM parameter $\tan\beta$ is 20. The simplified scenario includes gg-fusion, VBF, and VH production modes. The structures in the predicted curves arise because $\mathcal{B}(a_1 \to gg)$ varies rapidly as m_{a_1} crosses internal quark loop thresholds [46].

unshaded region, m_{h_1} is the independent variable and it is assumed that $m_{h_1} < m_{h_2}$, where m_{h_2} is the mass of the observed 125 GeV Higgs boson. In the shaded region where $m_{h_i} > 125$ GeV, m_{h_2} is the independent variable and it is assumed that m_{h_1} is the observed Higgs boson mass. In Fig. 2 (right), the sharp inflections in the reference line are due to the fact that $\mathcal{B}(a_1 \to 2\mu)$ is affected by the $a_1 \to s\bar{s}$ and $a_1 \to gg$ channels. As m_{a_1} crosses the internal quark loop thresholds, $\mathcal{B}(a_1 \to gg)$ changes rapidly, giving rise to structures in $\mathcal{B}(a_1 \to 2\mu)$ at these values of m_{a_1}. No hadronization effects are included in the $m_{a_1} < 2m_\tau$ region.

For the dark SUSY scenario, a 90% CL limit is set on the product of the Higgs boson production cross section and the branching fractions of the Higgs boson (cascade) decay to a pair of dark photons. The limit set by this experimental search is presented in Fig. 3 as areas excluded in a two dimensional plane of ε and m_{γ_D}. Also included in Fig. 3 are limits from other experimental searches [21, 61–74] including the most recent dark photon search result from LHCb [75]. For both this search and the ATLAS search, limits are shown for values of $\mathcal{B}(h \to 2\gamma_D + X)$ in the range 0.1–40%. The kinetic mixing parameter ε, the mass of the dark photon m_{γ_D}, and the life-

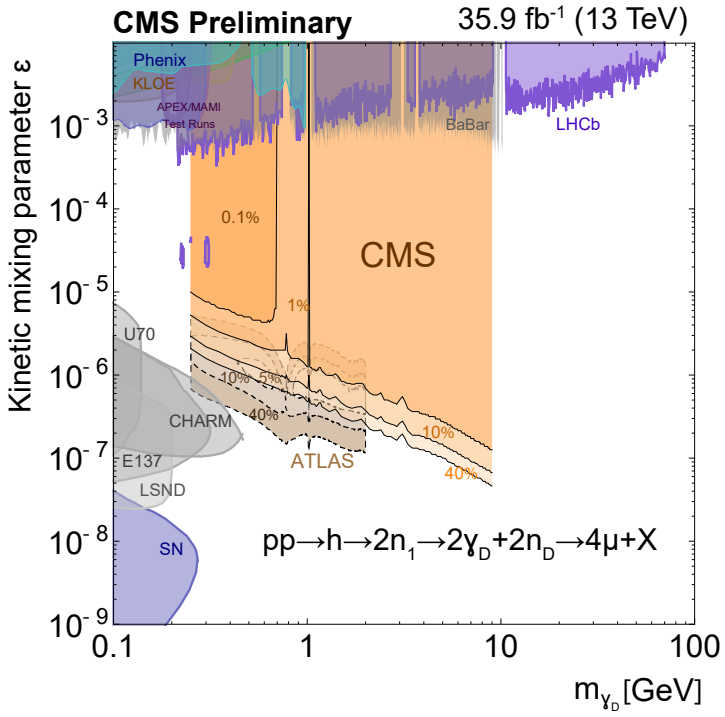

Figure 3: The 90% CL upper limits (black solid curves) from this search as interpreted in the dark SUSY scenario, where $\sigma(\mathrm{pp} \to \mathrm{h} + X)\,\mathcal{B}(\mathrm{h} \to 2\gamma_D + X)$ with $m_{\mathrm{n_1}} = 10\,\mathrm{GeV}$, $m_{\mathrm{n_D}} = 1\,\mathrm{GeV}$. The limits are presented in the plane of the parameters (ε and m_{γ_D}). Constraints from other experiments [21, 61–75] showing their 90% CL exclusion contours are also shown. The colored contours for the CMS and ATLAS limits represent different values of $\mathcal{B}(\mathrm{h} \to 2\gamma_D + X)$ that range from 0.1 to 40%.

time of the dark photon τ_{γ_D} are related via an analytic function $f(m_{\gamma_D})$ that is solely dependent on the dark photon mass [76]; namely, $\tau_{\gamma_D}(\varepsilon, m_{\gamma_D}) = \varepsilon^{-2} f(m_{\gamma_D})$. Due to the extensions of the range of these parameters, this search constrains a large and previously unconstrained area of the parameter space in ε and m_{γ_D}.

8 Summary

A search for pairs of new light bosons that subsequently decay to pairs of oppositely charged muons is presented in this Letter. This search is developed in the context of a Higgs boson decay, $\mathrm{h} \to 2\mathrm{a} + X \to 4\mu + X$ and is performed on a data sample collected by the CMS experiment in 2016 that corresponds to an integrated luminosity of $35.9\,\mathrm{fb}^{-1}$ proton-proton collisions with $\sqrt{s} = 13\,\mathrm{TeV}$. This dataset is larger and collected at a higher center-of-mass energy than the previous version of this search [15]. Additionally, both the mass range of the a boson and the maximum possible displacement of its decay vertex are extended compared to the previous publication of this analysis. Thirteen events are observed in the signal region, with $9.90 \pm 1.24\,(\mathrm{stat}) \pm 1.84\,(\mathrm{syst})$ events expected from the SM backgrounds. The distribution of events in the signal region is consistent with SM expectations. A model independent 95% CL upper limit on the product of the cross section, branching fraction, and acceptance is set over the mass range $0.25 < m_{\mathrm{a}} < 8.5\,\mathrm{GeV}$. This model independent limit is then interpreted in the context of dark SUSY with non-negligible light boson lifetime and the NMSSM. In the dark

SUSY interpretation of the result, the new limit constrains previously unexamined ranges of ε and m_{γ_D}.

References

[1] M. Maniatis, "The next-to-minimal supersymmetric extension of the standard model reviewed", *Int. J. Mod. Phys. A* **25** (2010) 3505, doi:10.1142/S0217751X10049827, arXiv:0906.0777.

[2] L. D. Duffy and K. van Bibber, "Axions as dark matter particles", *New J. Phys* **11** (2009) 105008, doi:10.1088/1367-2630/11/10/105008, arXiv:hep-ph/0904.3346.

[3] N. Arkani-Hamed, D. P. Finkbeiner, T. R. Slatyer, and N. Weiner, "A theory of dark matter", *Phys. Rev. D* **79** (2009) 015014, doi:10.1103/PhysRevD.79.015014, arXiv:0810.0713.

[4] A. Belyaev et al., "LHC discovery potential of the lightest NMSSM Higgs boson in the $h_1 \to a_1 a_1 \to 4\mu$ channel", *Phys. Rev. D* **81** (2010) 075021, doi:10.1103/PhysRevD.81.075021, arXiv:hep-ph/1002.1956.

[5] P. Fayet, "Supergauge invariant extension of the Higgs mechanism and a model for the electron and its neutrino", *Nucl. Phys. B* **90** (1975) 104, doi:10.1016/0550-3213(75)90636-7.

[6] R. K. Kaul and P. Majumdar, "Cancellation of quadratically divergent mass corrections in globally supersymmetric spontaneously broken gauge theories", *Nucl. Phys. B* **199** (1982) 36, doi:10.1016/0550-3213(82)90565-X.

[7] R. Barbieri, S. Ferrara, and C. A. Savoy, "Gauge models with spontaneously broken local supersymmetry", *Phys. Lett. B* **119** (1982) 343, doi:10.1016/0370-2693(82)90685-2.

[8] H. P. Nilles, M. Srednicki, and D. Wyler, "Weak interaction breakdown induced by supergravity", *Phys. Lett.* **120** (1983) 346, doi:10.1016/0370-2693(83)90460-4.

[9] J.-M. Frere, D. R. T. Jones, and S. Raby, "Fermion masses and induction of the weak scale by supergravity", *Nucl. Phys. B* **222** (1983) 11, doi:10.1016/0550-3213(83)90606-5.

[10] J.-P. Derendinger and C. A. Savoy, "Quantum effects and SU(2)×U(1) breaking in supergravity gauge theories", *Nucl. Phys. B* **237** (1984) 307, doi:10.1016/0550-3213(84)90162-7.

[11] M. Drees, "Supersymmetric models with extended Higgs sector", *Int. J. Mod. Phys. A* **4** (1989) 3635, doi:10.1142/S0217751X89001448.

[12] U. Ellwanger, C. Hugonie, and A. M. Teixeira, "The next-to-minimal supersymmetric standard model", *Phys. Rept.* **496** (2010) 1, doi:10.1016/j.physrep.2010.07.001, arXiv:0910.1785.

[13] M. Baumgart et al., "Non-abelian dark sectors and their collider signatures", *JHEP* **04** (2009) 014, doi:10.1088/1126-6708/2009/04/014, arXiv:0901.0283.

[14] A. Falkowski, J. T. Ruderman, T. Volansky, and J. Zupan, "Hidden Higgs decaying to lepton jets", *JHEP* **05** (2010) 077, doi:10.1007/JHEP05(2010)077, arXiv:1002.2952.

[15] CMS Collaboration, "A search for pair production of new light bosons decaying into muons", *Phys. Lett. B* **752** (2016) 146, doi:10.1016/j.physletb.2015.10.067, arXiv:1506.00424.

[16] ATLAS Collaboration, "Search for displaced muonic lepton jets from light Higgs boson decay in proton-proton collisions $\sqrt{s} = 7$ TeV with the ATLAS detector", *Phys. Lett. B* **721** (2013) 32, doi:10.1016/j.physletb.2013.02.058, arXiv:1210.0435.

[17] CMS Collaboration, "Search for light resonances decaying into pairs of muons as a signal of new physics", *JHEP* **07** (2011) 98, doi:10.1007/JHEP07(2011)098, arXiv:1106.2375.

[18] CMS Collaboration, "Search for a very light NMSSM Higgs boson produced in decays of the 125 GeV scalar boson and decaying into τ leptons in pp collisions at $\sqrt{s} = 8$ TeV", *JHEP* **01** (2016) 079, doi:10.1007/JHEP01(2016)079, arXiv:1510.06534.

[19] ATLAS Collaboration, "Search for new light gauge bosons in Higgs boson decays to four-lepton final states in pp collisions at $\sqrt{s} = 8$ TeV with the ATLAS detector at the LHC", *Phys. Rev. D* **92** (2015) 092001, doi:10.1103/PhysRevD.92.092001, arXiv:1505.07645.

[20] ATLAS Collaboration, "Search for Higgs boson decays to beyond-the-Standard-Model light bosons in four-lepton events with the ATLAS detector at $\sqrt{s} = 13$ TeV", (2018). arXiv:1802.03388. Submitted to *JHEP*.

[21] ATLAS Collaboration, "Search for long-lived neutral particles decaying into lepton jets in proton–proton collisions at $\sqrt{s}$ = 8 TeV with the ATLAS detector", *JHEP* **11** (2014) 88, doi:10.1007/JHEP11(2014)088, arXiv:1409.0746.

[22] ATLAS Collaboration, "Search for the Higgs boson produced in association with a W boson and decaying to four b-quarks via two spin-zero particles in pp collisions at 13 TeV with the ATLAS detector", *Eur. Phys. J. C* **76** (2016) 605, doi:10.1140/epjc/s10052-016-4418-9, arXiv:1606.08391.

[23] ATLAS Collaboration, "Search for the Higgs boson produced in association with a vector boson and decaying into two spin-zero particles in the $H \to aa \to 4b$ channel in pp collisions at $\sqrt{s} = 13$ TeV with the ATLAS detector", (2018). arXiv:1806.07355. Submitted to *JHEP*.

[24] ATLAS Collaboration, "Search for new phenomena in events with at least three photons collected in pp collisions at $\sqrt{s}$ = 8 TeV with the ATLAS detector", *Eur. Phys. J. C* **76** (2016) 210, doi:10.1140/epjc/s10052-016-4034-8, arXiv:1509.05051.

[25] CMS Collaboration, "Search for the exotic decay of the Higgs boson to a pair of light pseudoscalars in the final state with two b quarks and two τ leptons", (2018). arXiv:1805.10191. Submitted to *Phys. Lett. B*.

[26] CMS Collaboration, "Search for the exotic decay of the Higgs boson to a pair of light pseudoscalars in the final state of two muons and two τ leptons at $\sqrt{s} = 13$ TeV", (2018). arXiv:1805.04865. Submitted to *JHEP*.

[27] LHCb Collaboration, "Search for Higgs-like bosons decaying into long-lived exotic particles", *The Eur. Phys. J. C* **76** (2016) 664, doi:10.1140/epjc/s10052-016-4489-7, arXiv:1609.03124.

[28] CMS Collaboration, "Search for a non-standard-model Higgs boson decaying to a pair of new light bosons in four-muon final states", *Phys. Lett. B* **726** (2013) 564, doi:10.1016/j.physletb.2013.09.009, arXiv:1210.7619.

[29] CMS Collaboration, "Performance of the CMS muon detector and muon reconstruction with proton-proton collisions at $\sqrt{s} = 13$ TeV", (2018). arXiv:1804.04528. Submitted to *JINST*.

[30] CMS Collaboration, "Performance of CMS muon reconstruction in pp collision events at $\sqrt{s} = 7$ TeV", *JINST* **7** (2012) P10002, doi:10.1088/1748-0221/7/10/P10002, arXiv:1206.4071.

[31] CMS Collaboration, "The CMS trigger system", *JINST* **12** (2017) P01020, doi:10.1088/1748-0221/12/01/P01020, arXiv:1609.02366.

[32] CMS Collaboration, "The CMS experiment at the CERN LHC", *JINST* **3** (2008) S08004, doi:10.1088/1748-0221/3/08/S08004.

[33] CMS Collaboration, "Particle-flow reconstruction and global event description with the CMS detector", *JINST* **12** (2017) P10003, doi:10.1088/1748-0221/12/10/P10003, arXiv:1706.04965.

[34] W. Adam, B. Mangano, T. Speer, and T. Todorov, "Track reconstruction in the CMS tracker", Technical Report CMS-NOTE-2006-041, CERN, Geneva, 2006.

[35] NNPDF Collaboration, "Parton distributions with QED corrections", *Nucl. Phys. B* **877** (2013) 290–320, doi:10.1016/j.nuclphysb.2013.10.010, arXiv:1308.0598.

[36] T. Sjöstrand et al., "An introduction to PYTHIA 8.2", *Computer Physics Communications* **191** (2015) 159, doi:10.1016/j.cpc.2015.01.024, arXiv:1410.3012.

[37] P. Skands, S. Carrazza, and J. Rojo, "Tuning PYTHIA 8.1: the Monash 2013 tune", *Eur. Phys. J. C* **74** (2014) 3024, doi:10.1140/epjc/s10052-014-3024-y, arXiv:1404.5630.

[38] WMAP Collaboration, "Nine-year Wilkinson microwave anisotropy probe (WMAP) observations: Cosmological parameter results", *Astrophys. J. Suppl.* **208** (2013) 19, doi:10.1088/0067-0049/208/2/19, arXiv:1212.5226.

[39] Planck Collaboration, "Planck 2013 results. XVI. Cosmological parameters", *Astron. Astrophys.* **571** (2014) A16, doi:10.1051/0004-6361/201321591, arXiv:1303.5076.

[40] OPAL Collaboration, "Decay mode independent searches for new scalar bosons with the OPAL detector at LEP", *Eur. Phys. J. C* **27** (2003) 311, doi:10.1140/epjc/s2002-01115-1, arXiv:hep-ex/0206022.

[41] OPAL Collaboration, "Search for a low mass CP-odd Higgs boson in e^+e^- collisions with the OPAL detector at LEP-2", *Eur. Phys. J. C* **27** (2003) 483, doi:10.1140/epjc/s2003-01139-y, arXiv:hep-ex/0209068.

[42] ALEPH, DELPHI, L3, OPAL, LEP Working Group for Higgs Boson Searches Collaboration, "Search for neutral MSSM Higgs bosons at LEP", *Eur. Phys. J. C* **47** (2006) 547, doi:10.1140/epjc/s2006-02569-7, arXiv:hep-ex/0602042.

[43] OPAL Collaboration, "Search for neutral Higgs boson in CP-conserving and CP-violating MSSM scenarios", *Eur. Phys. J. C* **37** (2004) 49, doi:10.1140/epjc/s2004-01962-6, arXiv:hep-ex/0406057.

[44] DELPHI Collaboration, "Searches for neutral Higgs bosons in extended models", *Eur. Phys. J. C* **38** (2004) 1, doi:10.1140/epjc/s2004-02011-4, arXiv:hep-ex/0410017.

[45] ALEPH Collaboration, "Search for neutral Higgs bosons decaying into four taus at LEP2", *JHEP* **05** (2010) 049, doi:10.1007/JHEP05(2010)049, arXiv:1003.0705.

[46] R. Dermisek and J. F. Gunion, "New constraints on a light CP-odd Higgs boson and related NMSSM ideal Higgs scenarios", *Phys. Rev. D* **81** (2010) 075003, doi:10.1103/PhysRevD.81.075003, arXiv:1002.1971.

[47] J. Alwall et al., "MadGraph/MadEvent v4: the new web generation", *JHEP* **09** (2007) 028, doi:10.1088/1126-6708/2007/09/028, arXiv:0706.2334.

[48] P. Meade and M. Reece, "BRIDGE: Branching ratio inquiry / decay generated events", arXiv:hep-ph/0703031.

[49] GEANT4 Collaboration, "GEANT4—a simulation toolkit", *Nucl. Instrum. Meth. A* **506** (2003) 250, doi:10.1016/S0168-9002(03)01368-8.

[50] CMS Collaboration, "Search for supersymmetry in pp collisions at $\sqrt{s} = 13$ TeV in the single-lepton final state using the sum of masses of large-radius jets", *JHEP* **08** (2016) 122, doi:10.1007/JHEP08(2016)122, arXiv:1605.04608v2.

[51] T. Sjöstrand, S. Mrenna, and P. Z. Skands, "A brief introduction to PYTHIA 8.1", *Comput. Phys. Commun.* **178** (2008) 852, doi:10.1016/j.cpc.2008.01.036, arXiv:0710.3820.

[52] M. Bahr et al., "Herwig++ physics and manual", *Eur. Phys. J. C* **58** (2008) 639, doi:10.1140/epjc/s10052-008-0798-9, arXiv:0803.0883.

[53] A. Belyaev, N. D. Christensen, and A. Pukhov, "CalcHEP 3.4 for collider physics within and beyond the standard model", *Comput. Phys. Commun.* **184** (2013) 1729, doi:10.1016/j.cpc.2013.01.014, arXiv:1207.6082.

[54] CMS Collaboration, "CMS luminosity measurements for the 2016 data taking period", CMS Physics Analysis Summary CMS-PAS-LUM-17-001, 2017.

[55] M. Botje et al., "The PDF4LHC working group interim recommendations", arXiv:1101.0538.

[56] S. Alekhin et al., "The PDF4LHC working group interim report", arXiv:1101.0536.

[57] R. D. Ball et al., "Parton distributions with LHC data", *Nucl. Phys. B* **867** (2013) 244, doi:10.1016/j.nuclphysb.2012.10.003, arXiv:1207.1303.

[58] J. Butterworth et al., "PDF4LHC recommendations for LHC Run II", *J. Phys. G: Nucl. Part. Phys.* **43** (2016) 023001, arXiv:1510.03865v2.

[59] J. M. Campbell and R. Ellis, "Loops and legs in quantum field theory MCFM for the Tevatron and the LHC", *Nucl. Phys. B Proc. Suppl.* **205** (2010) 10, doi:10.1016/j.nuclphysbps.2010.08.011, arXiv:1007.3492v1.

[60] LHC Higgs Cross Section Working Group Collaboration, "Handbook of LHC Higgs cross sections: 1. inclusive observables", doi:10.5170/CERN-2011-002, arXiv:1101.0593.

[61] PHENIX Collaboration, "Search for dark photons from neutral meson decays in $p+p$ and $d+$Au collisions at $\sqrt{s_{NN}} = 200$GeV", *Phys. Rev. C* **91** (2015) 031901, doi:10.1103/PhysRevC.91.031901, arXiv:1409.0851.

[62] KLOE-2 Collaboration, "Search for light vector boson production in $e^+e^- \to \mu^+\mu^-\gamma$ interactions with the KLOE experiment", *Phys. Lett. B* **736** (2014) 459, doi:10.1016/j.physletb.2014.08.005, arXiv:1404.7772.

[63] APEX Collaboration, "Search for a new gauge boson in electron-nucleus fixed-target scattering by the APEX Experiment", *Phys. Rev. Lett.* **107** (2011) 191804, doi:10.1103/PhysRevLett.107.191804, arXiv:1108.2750.

[64] A. Adare et al., "Search at the Mainz Microtron for light massive gauge bosons relevant for the muon g-2 anomaly", *Phys. Rev. Lett.* **112** (2014) 221802, doi:10.1103/PhysRevLett.112.221802, arXiv:1404.5502.

[65] HADES Collaboration, "Searching a dark photon with HADES", *Phys. Lett. B* **731** (2014) 265, doi:10.1016/j.physletb.2014.02.035, arXiv:1311.0216.

[66] BaBar Collaboration, "Search for a dark photon in e+e- collisions at BABAR", *Phys. Rev. Lett.* **113** (2014) 201801, doi:10.1103/PhysRevLett.113.201801, arXiv:1406.2980.

[67] A. Fradette, M. Pospelov, J. Pradler, and A. Ritz, "Cosmological constraints on very dark photons", *Phys. Rev. D* **90** (2014) 035022, doi:10.1103/PhysRevD.90.035022, arXiv:1407.0993.

[68] R. Essig et al., "Working group report: New light weakly coupled particles", arXiv:1311.0029.

[69] L. M. K. James B. Dent, Francesc Ferrer, "Constraints on light hidden sector gauge bosons from supernova cooling", arXiv:1201.2683.

[70] H. K. Dreiner, J. Fortin, and L. U. C. Hanhart, "Supernova constraints on MeV dark sectors from e+ e- annihilations", *Phys. Rev. D* **89** (2014) 105015, doi:10.1103/PhysRevD.89.105015, arXiv:1310.3826.

[71] J. B. J. Blumlein, "New exclusion limits for dark gauge forces from beam-dump data", *Phys. Lett. B* **701** (2011) 155, doi:10.1016/j.physletb.2011.05.046, arXiv:1104.2747.

[72] R. Essig, R. Harnik, J. Kaplan, and N. Toro, "Discovering new light states at neutrino experiments", *Phys. Rev. D* **82** (2010) 113008, doi:10.1103/PhysRevD.82.113008, arXiv:1008.0636.

[73] A. R. Brian Batell, Maxim Pospelov, "Exploring portals to a hidden sector through fixed targets", *Phys. Rev. D* **80** (2009) 095024, doi:10.1103/PhysRevD.80.095024, arXiv:0906.5614.

[74] S. N. Gninenko, "Constraints on sub-GeV hidden sector gauge bosons from a search for heavy neutrino decays", *Phys. Lett. B* **713** (2012) 244, doi:10.1016/j.physletb.2012.06.002, arXiv:1204.3583.

[75] LHCb Collaboration, "Search for dark photons produced in 13 TeV pp collisions", *Phys. Rev. Lett.* **120** (2018) 061801, doi:10.1103/PhysRevLett.120.061801, arXiv:1710.02867.

[76] B. Batell, M. Pospelov, and A. Ritz, "Probing a secluded U(1) at B-factories", *Phys. Rev. D* **79** (2009) 115008, doi:10.1103/PhysRevD.79.115008, arXiv:0903.0363.